COBEM 2021 26th International Congress of Mechanical Engineering
ABCM Associação Brasileira de Engenharia e Ciências Mecânicas
November 22-26, 2021, Virtual Congress, Brazil

COBEM2021-0695
THERMAL AND HYDRODYNAMIC BEHAVIOR OF A MICRO-FINNED HEAT SINK FOR CONVECTIVE FLOW BOILING OF DIELECTRIC FLUID

Jéssica Martha Nunes[1]
Willy Kelton Nóbrega Azevedo[1]
[1]UNESP - Universidade Estadual Paulista/Faculdade de Engenharia - Câmpus de Ilha Solteira, Av. Brasil Sul, 56 - Centro, Ilha Solteira.
jessica.nunes@unesp.br
willy.azevedo@unesp.br

Elaine Maria Cardoso[1,2]
[1]UNESP - Universidade Estadual Paulista/Faculdade de Engenharia - Câmpus de Ilha Solteira, Av. Brasil Sul, 56 - Centro, Ilha Solteira.
[2]UNESP - Universidade Estadual Paulista/Câmpus de São João da Boa Vista, Av. Profa. Isette Correa Fontão, 505 - Jardim das Flores, São João da Boa Vista – SP, 13876-750
elaine.cardoso@unesp.br

Abstract. *It is notable the advancement in the high-power electronics development and the miniaturization of devices, requiring higher levels of energy dissipation. This work evaluates a micro-finned heat sink's thermal and hydrodynamic behavior, using convective flow boiling of the HFE-7100. Square micro-pin fins with 160 µm in height were manufactured on a copper surface through the micro-milling process. The pressure drop and surface temperature behavior were analyzed for different mass fluxes (800, 1000 and 1200 kg/m²s) and inlet subcooling (10 and 20 °C). The effect of mass flux on the heat transfer coefficient (HTC) is negligible for the inlet subcooling of 10 ºC; in the case of 20 °C, an increase in mass flux causes an enhancement in the HTC for low to moderate heat flux; by increasing heat flux, the HTC is no longer influenced by the mass flux, showing the gradual control of boiling over convection as the main heat transfer mechanism. The pressure drop increases exponentially with the heat flux in the two-phase flow regime as the vapor generation rate becomes pronounced. Besides, decreasing the inlet subcooling increases the pressure drop at the same heat flux, where the lowest inlet subcooling results in a higher vapor quality along the heat sink, leading to a more significant pressure drop.*

Keywords: *two-phase flow, convective heat transfer, pressure drop, micro-pin fin, HFE-7100.*

1. INTRODUCTION

Due to the continuous search for increasing the processing capacity of high-powered electronic devices, the challenge is to develop heat dissipation alternatives that could meet the cooling demand of such high-performance processors. US Department of Energy surveys project that by 2030, more than 80% of all electricity will flow through some electronic power circuit in the US (Power America, 2014). Power electronics are used for different applications such as photovoltaic panels, high-performance computers, smart grids, hybrid electric vehicles, military fighter jets, and industrial automation. The electronics miniaturization coupled with an increase in processing capacity leads to the increase of heat generation rate. Thus, new thermal management solutions are needed to ensure the component's physical integrity and perfect functioning.

Convective boiling heat transfer in microchannels has been one solution for an effective cooling solution and has received attention in recent years due to its ability to dissipate high heat fluxes; HTC enhancement was observed by using microchannels, mainly for higher inlet subcooling. However, as the vapor quality increased along the microchannels, flow boiling instabilities may arise and flow reversal can occur, affecting the heat transfer performance (Kadam and Kumar, 2014; Kandlikar, 2016; Prajapati *et al*., 2017). Therefore, new surface structures were developed to solve flow instabilities and improve heat transfer performance.

One suggested technique was modifying the channel surface area through divergent cross-sectional microchannels (Mukherjee and Kandlikar, 2005; Lee and Pan, 2008; Fu *et al*., 2012) and segmented microchannels or micro-pin fins (Figure 1). In the segmented microchannel system, the main channels are cut by the secondary channels; due to these interconnections, the regeneration of the thermal and hydraulic boundary layers is facilitated throughout the refrigerant fluid flow. In addition, microfins provide more significant heat transfer in the convective boiling regime since they increase the heat transfer area and promote more active nucleation sites. The optimum pin-fin length scales depend on

the working fluid and its subcooling in the system. As indicated by McNeil *et al*. (2014), mini and micro pin-fin arrangements are promising surface structures for compact heat sinks.

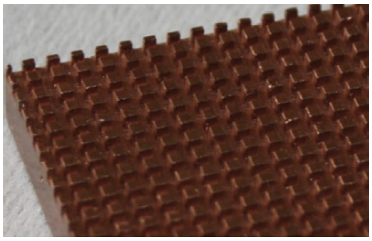

Figure 1. Example of segmented microchannels (micro-pin fins) (McNeil *et al*., 2014).

Jiang *et al*. (2002) initially proposed a segmented microchannel consisting of 18 parallel microchannels with 150 μm hydraulic diameter interconnected with 5 transverse slots, with 100 μm width. Due to the lateral fluid flow, better surface temperature uniformity was observed under non-uniform heating conditions. Later, Xu *et al*. (2006) experimentally and numerically investigated the hydrodynamic and thermal behavior of an interconnected microchannel heat sink. In the two-phase flow boiling, isolated bubbles occurred near the interconnected region (*i.e.,* more nucleation sites), which led to a uniform temperature distribution on the surface. Mihailovic *et al*. (2011) carried out experimental tests of convective boiling of deionized water in finned microchannels. For low fluid flow rates (1 to 5 ml/h), the micro-finned channels were efficient in suppressing the reverse flow, significantly reducing system instabilities; a flow rate of 5 ml/h made it possible to dissipate a heat flux of up to 40 W/cm² with this heat sink configuration. In addition, Reeser *et al*. (2014) investigated the convective boiling heat transfer using micro-pin fins fabricated in two different arrays: aligned and staggered. They used deionized water and HFE-7200 as working fluids, with a vapor quality of up to 90% at the heat sink outlet. According to them, an HTC augmentation of 50% was observed for the staggering array and HFE-7200. On the other hand, the pressure loss was on average 50% higher than the aligned one, both for HFE-7200 and deionized water.

Recently, Deng *et al*. (2021) studied a type of advanced microchannels consisting of two small inner rings enclosing a cavity for vapor bubbles nucleation and two larger outer rings, with separate and converging flow passages. The authors worked with a subcooled (10 °C) two-phase flow of deionized water in two micro-pin fin arrays: aligned and staggered. The aligned array showed an increase of 10 to 80% in HTC for moderate and high heat fluxes, 2 to 20% lower pressure drop, and a more stable flow than the staggered array. Such results were attributed to the difficulty of the coalesced vapor bubbles to flow between the staggered micro fins for moderate to high heat fluxes (for the aligned array, there is a “corridor” through which these coalesced bubbles can flow, without significant resistance). Similarly, Asrar, Ghiaasiaan and Joshi (2021) experimentally investigated the convective boiling of R245fa in micro gaps improved with cylindrical micro-pin fins; different conditions of mass flux (G) and inlet temperatures were tested. For the single-phase flow regime, the HTC increased with increasing G; and, for the two-phase flow regime, the HTC increased with the temperature. Regarding pressure drop and vapor quality, Asrar, Ghiaasiaan and Joshi (2021) found the same as Woodcock *et al*. (2015) and Chien *et al*. (2020), where these two parameters drastically increased with the intensification of convective boiling.

In this context, this study aims to experimentally analyze the convective flow boiling of dielectric fluid, HFE-7100 with different inlet conditions, in compact heat sinks based on segmented microchannels or micro-pin fins with an aligned array. The thermal and hydrodynamic behaviors were analyzed for different mass fluxes (800, 1000 and 1200 kg/m²s) and inlet subcooling (10 and 20 °C), including the flow visualization.

2. MATERIALS AND METHODS

2.1 Micro-finned heat sink fabrication and characterization

The heat sink (Figure 2.a) consists of a copper block with a 20 x 15 mm footprint area. Square micro-pin fins (D = 300 μm in width, H = 160 μm in height, and S = 250 μm of distance between the fins) were manufactured using a CNC precision milling machine (Hermile, model C800U). The micro fins were manufactured in an aligned array with the fluid flow direction (Figure 2.b).

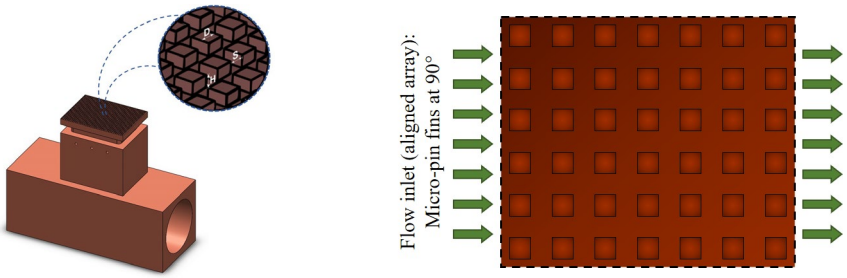

(a) (b)

Figure 2. (a) Scheme of the copper block with micro-pin fins; (b) Constructive array of the micro-pin fins.

The heat sink has 972 micro-pin fins corresponding to an effective roughness (R_{eff}) of 1.63. The R_{eff} is defined as the ratio between the area in contact with the working fluid and the projected area (Dong *et al.*, 2014).

The characterization of the micro-finned heat sink was performed using two microscopy techniques (geometric characterization by Zeiss® SteREO DiscoveryV8 and SEM EVO LS15 Zeiss®, Table 1) and a fluid/surface interaction characterization (capillary wicking behavior).

Table 1. Structural characterization of the micro-finned heat sink.

Stereo		SEM
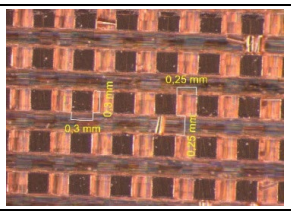	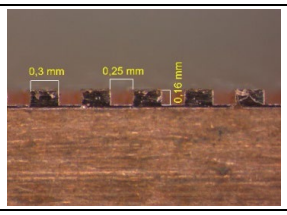	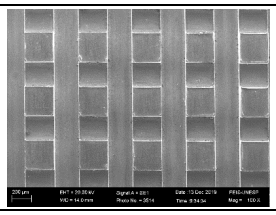

The capillary wicking behavior was evaluated for HFE-7100 at room temperature (20 ºC). Different authors (Rahman et al., 2014; Cao et al., 2018; Kiyomura et al., 2020; Manetti et al., 2020) carried out a capillary-wicking test where the test surface is slowly raised to contact a pendant fluid droplet attached to a small diameter capillary tube. As the surface contacts the liquid droplet, the fluid is wicked into the structure and the volumetric flow rate is measured by monitoring the liquid meniscus in the tube. The capillary tube used in the current study had 1 mm in diameter. More details about the procedure can be found in Kiyomura et al. (2020) and Manetti et al. (2020). As a result, the micro-finned heat sink can absorb more liquid than a plain surface (used as a reference surface).

2.2 Apparatus assembly

Figure 3 shows the design of the heat sink test section in different views, including a cutaway to view internal details and element descriptions (Figure 3.b). Five holes (1 mm diameter) were drilled in the copper block to accommodate K-type thermocouples (A) to determine the wall temperature and verify the one-dimensional heat conduction along the copper block. The heat flux is provided by electrical resistance (cartridge type, 250 W/220 V) embedded in the copper block (B) and controlled by a DC power supply.

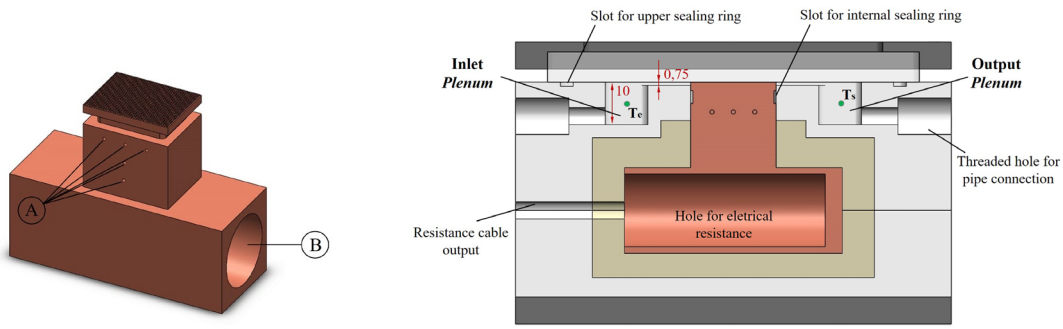

(a) (b)

Figure 3. Design of the micro-finned heat sink. (a) Isometric view; (b) Front view with internal details (measurements in mm).

The test section is thermally insulated with refractory ceramic and polytetrafluoroethylene (PTFE). The inlet and outlet plenums were machined on the PTFE; thus, the working fluid was not heated before contacting the segmented inlet channels of the heat sink. The plenums were manufactured with 10 x 15 x 10 mm and two K-type thermocouples, one in the inlet and another in the outlet, measure the working fluid temperature (T_e and T_s, respectively). Between the plenums and the test surface, flow homogenization channels with a depth of 0.75 mm were manufactured to minimize flow entrance turbulence. A polycarbonate plate (2 mm thickness) covers the heat sink to allow flow visualization.

Figure 4 presents a schematic diagram of the experimental apparatus. The working fluid was pumped from a fluid reservoir to the flow loop; the HFE7100 flow rate was set by a Coriolis mass flow meter (Yokogawa ROTAMASS Total Insight with 0.2 % mass flow accuracy) installed just upstream the pre-heater (consisted of a horizontal copper tube heated by an electrical tape resistance). There is a bypass line used for the test facility maintenance. The pressure drop between inlet and outlet plenums was measured by two pressure transducers (OMEGA PX309 model assuming its uncertainty equal to that given by the manufacturer, 0.4 kPa). The flow temperature was measured using previously calibrated K-type thermocouples in the inlet and outlet plenums (both in contact with the fluid). The working fluid was cooled by a condenser and then returned to the reservoir.

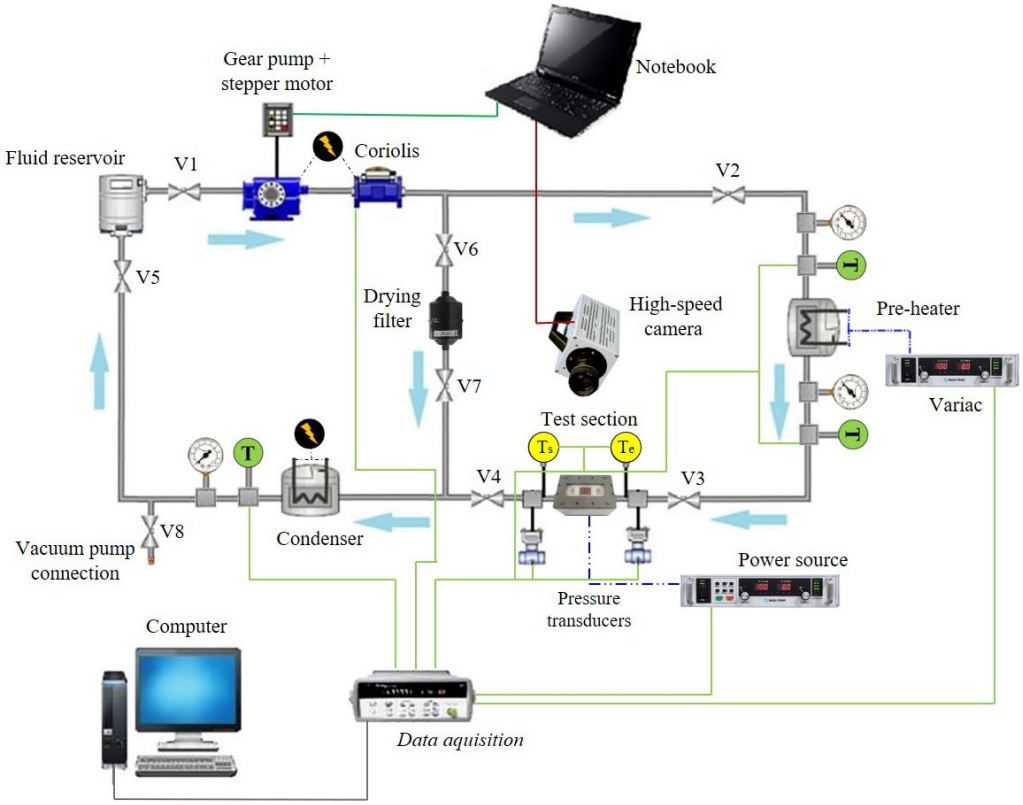

Figure 4. Schematic diagram of the experimental apparatus.

The method described in Figliola and Beasley (2006) was used to calculate the heat flux and heat transfer uncertainties. Consequently, the uncertainty of the heat flux and the heat transfer coefficient varied from 2 to 10 % and from 3 to 12.6 %, respectively.

2.3 Experimental procedure

The validation verifies the coherence of the results obtained experimentally; thus, it was performed in a single-phase regime to compare the experimental data with known correlations from literature. After the validation, two-phase flow tests were performed for two different subcooling values, 10 ºC and 20 ºC; mass fluxes of 800, 1000 and 1200 kg/m²; and, for different footprint heat fluxes from 10 kW/m² to the system limit, characterized by intense instability in the flow (reverse flow). The rpm of the gear pump was set such that the desired mass flux was achieved; the preheater was adjusted until its outlet temperature was equal to the desired subcooling. A data acquisition system (Agilent 34970A) recorded the data every 10 seconds after the system achieved the steady-state regime, characterized by temperature variations lower than the experimental thermocouples uncertainties (± 0.3 °C). The pressure, fluid and copper block temperatures, mass flux, the electrical voltage in the cartridge heater and pre-heater resistance are constantly monitored. Flow visualization was carried out using a high-speed camera (Photron FASTCAM SA3 with a

100 mm lens and 1024 × 1024 maximum resolution and 1000 fps). The same procedure was adopted during all the experimental tests in order to ensure repeatability.

2.3.1 Data reduction

Heat Transfer Coefficient (HTC), h:

The heat transfer coefficient is calculated based on Eqs. (1) - (7), similarly to the approach adopted by Prajapati *et al*. (2017).

$$Q_{loss} = Q_{in} - \dot{m} \cdot c_p(T_s - T_e) \tag{1}$$

where $\dot{m}$ corresponds to the mass flow rate [kg/s]; c_p to the specific heat capacity [J/kg·K]; T_e and T_s to the coolant temperature at the inlet and outlet, respectively. In the current study. the heat loss (Q_{loss}) varied from 15 to 30% over the range of varying parameters. The heat flux, q'', dissipated by the test section is given by Eq. (2):

$$q'' = \frac{(Q_{in} - Q_{loss})}{A_p} \tag{2}$$

where A_p is the footprint area of the heating surface. The effective heat flux, q''_{eff} [W/m²], based on the total surface area in contact with the working fluid (A_t), is calculated by Eq. (3):

$$q''_{eff} = \frac{(Q_{in} - Q_{loss})}{A_t} \tag{3}$$

In order to calculate the total surface area, A_t, the fin parameters and efficiency concepts have been calculated considering the adiabatic fin tip since a polycarbonate plate is used to cover the heat sink.

$$m = \sqrt{\frac{h \cdot P_{ma}}{k_c \cdot A_c}} \qquad \eta = \frac{tanh(m \cdot H)}{m \cdot H} \tag{4}$$

where h is the experimental heat transfer coefficient [W/m²·K]; P_{ma} is the micro-pin fin perimeter; k_c is the thermal conductivity of copper [W/m·K]; A_c is the cross-sectional area, and H is the height of the micro-pin fins. Thus, A_t is given by Eq. (5), where N is the total number of micropillars.

$$A_t = \left(A_p - N \cdot A_c\right) + \eta \cdot N \cdot P_{ma} \cdot H \tag{5}$$

Therefore, it is possible to calculate the heat transfer coefficient (h) through Newton's cooling law, given by Eq. (6), where T_w is the average temperature of the heat sink given by three K-type thermocouples fixed within the heat sink wall, and the T_f is the average temperature of the fluid given by the same procedure as Leão, Nascimento and Ribastki (2014).

$$h = \frac{q''_{eff}}{T_w - T_f} \tag{6}$$

Pressure drop, Δp:

Pressure transducers (at inlet and outlet plenums, P_i and P_e, respectively) measure the pressure drop in the region between the inlet and outlet plenums; thus, the pressure drop through the microchannels is given by $\Delta P = (P_i - P_e) - \Delta P_{contraction} - \Delta P_{expansion}$ where the pressure drop due to contraction and expansion are obtained by the method described in Chalfi and Ghiaasiaan (2008).

3. RESULTS AND DISCUSSION

3.1 Effect of the mass flux

Figure 5 shows the effect of different mass fluxes on the boiling curves and HTC curves of HFE-7100 for different inlet subcooling temperatures (10 and 20 °C).

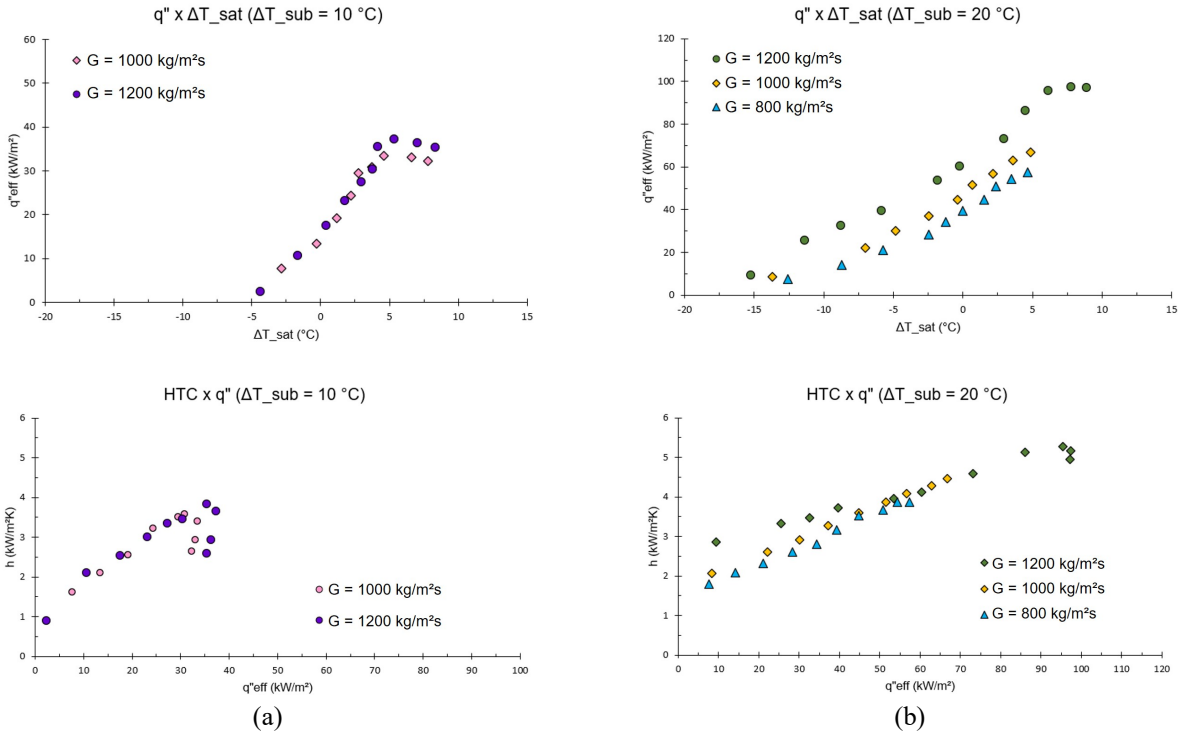

(a) (b)

Figure 5. Effect of mass flux on convective flow boiling heat transfer of HFE-7100. (a) ΔT_{sub} = 10 ºC; (b) ΔT_{sub} = 20 ºC.

The influence of mass flux, G, on the convective flow boiling heat transfer was negligible for the inlet subcooling of 10°C, showing a slight increase in the HTC and dryout heat flux for G = 1200 kg/m²s (Figure 5.a); for the inlet subcooling of 20 ºC (Figure 5.b), an increase in the mass flux shifted the curves to the left, for low to moderate heat fluxes, characterized by an HTC enhancement. Cheng and Wu (2021) indicated a gradual predominance of boiling heat transfer over convection as heat flux increases, which was also previously reported by Harirchian and Garimella (2008). Moreover, as Yin et al. (2020) mentioned, the micro-pin fins induced flow turbulence and strengthened convection heat transfer, the main heat dissipation component in subcooled convective boiling.

In addition, for ΔT_{sub} = 20 ºC, an HTC degradation was observed for higher heat fluxes (being more pronounced for G = 1200 kg/m²s). According to Dalkiliç *et al*. (2018), this is due to the dryout hot spots leading to a heat transfer deterioration.

3.2 Effect of the inlet subcooling temperature

Figure 6 shows the effect of different inlet subcooling temperatures (10 and 20 ºC) on the boiling heat transfer performance. An increase in the subcooling shifted the boiling curve to the left. According to Yin *et al*. (2020), a lower inlet subcooling temperature facilitates the nucleate boiling and heat transfer evaporation; however, they observed the HTC continuously increasing with heat flux for all mass fluxes values and higher inlet subcooling temperature, while the HTC decreased with high heat fluxes for lower inlet subcooling temperature. Yin *et al*. (2020) attributed this behavior to flow pattern transition into confined annular flow, where partial dryout occurs on the surface as heat flux increases, leading to a sharp increase in the surface temperature and a decrease in the slope of the boiling curves, as shown in Figure 6.

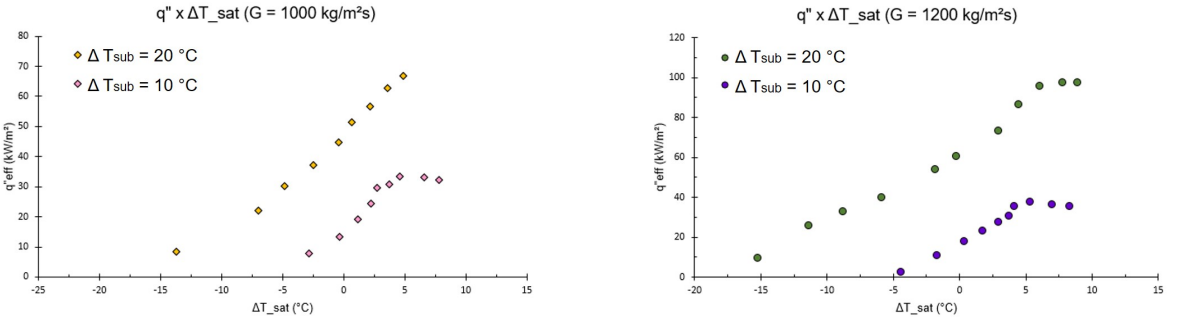

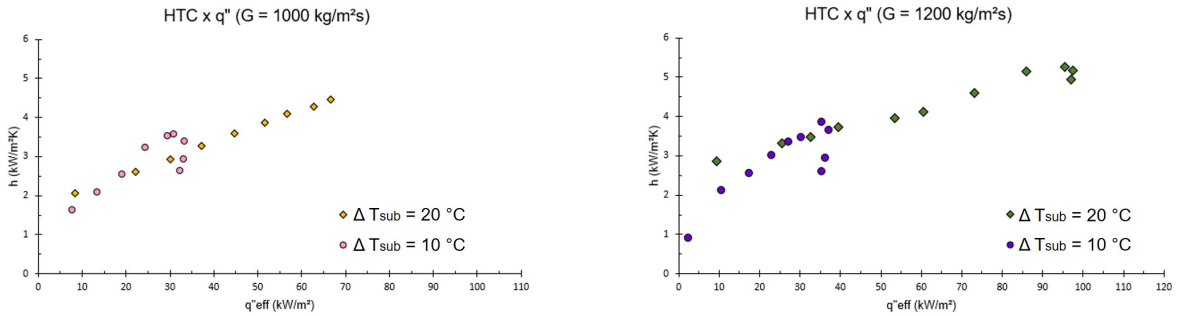

(a) (b)

Figure 6. Effect of inlet subcooling temperature on convective flow boiling heat transfer of HFE-7100. (a) G = 1000 kg/m²s; (b) G = 1200 kg/m²s.

The boiling hysteresis phenomena characterized by a large wall temperature excursion, usually found in boiling incipience for conventional microchannels, was not observed in the current study.

3.3 Pressure drop

Figure 7 shows the effect of inlet subcooling temperature on pressure drop. For two-phase flow region, as the inlet subcooling temperature decreased, the pressure drop became larger, at the same heat flux value and regardless of the mass flux (a lower inlet subcooling temperature of the fluid results in a higher vapor quality along the heat sink, leading to a more significant pressure drop as also observed by Yin *et al*. (2020) and Cheng and Wu (2021)). Similarly, Dang *et al.* (2020) reported that the pressure drop increases as the vapor quality gradually increases with heat flux (the shear stress at the liquid-vapor interface is higher, resulting in the friction pressure drop enhancement).

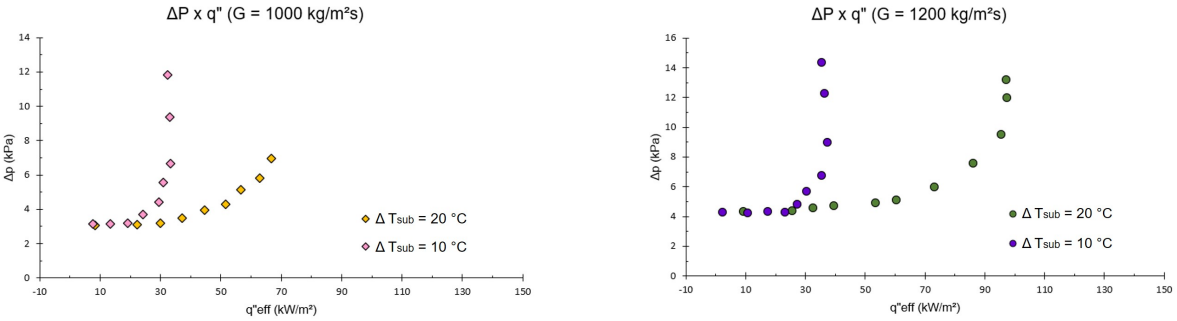

(a) (b)

Figure 7. Effect of inlet subcooling temperatures on the pressure drop. (a) G = 1000 kg/m²s; (b) G = 1200 kg/m²s.

Figure 8 shows the effect of mass flux on pressure drop. An increase in mass flux leaded to an increase in the pressure drop for low heat fluxes (< 25 kW/m² for ΔT_{sub} = 10 ºC; and, < 45 kW/m² for ΔT_{sub} = 20 ºC). As the heat flux increased, the pressure drop became more pronounced due to the increase in the vapor mass flowing through the heat sink. No significant influence of mass flux on pressure drop was observed in the two-phase flow region for both inlet subcooling temperatures (10 and 20 ºC).

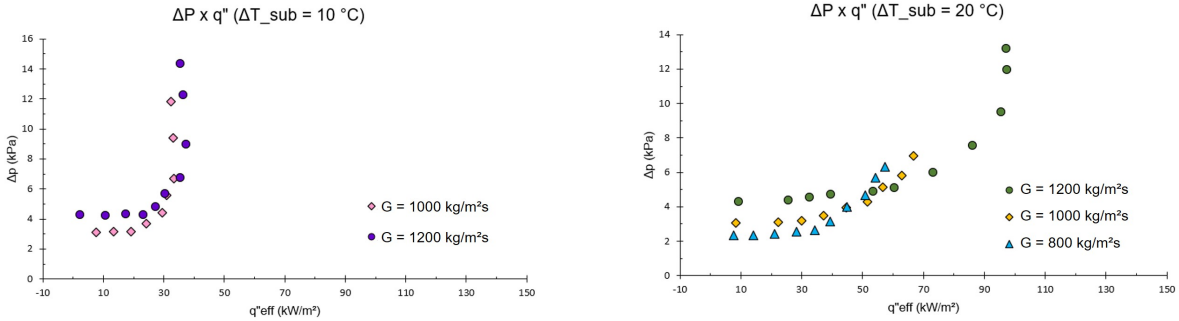

(a) (b)

Figure 8. Effect of mass flux on pressure drop. (a) ΔT_{sub} = 10 ºC; (b) ΔT_{sub} = 20 ºC.

3.4 Flow visualization

The visualization indicated that isolated vapor bubbles were formed between the adjacent pin fins (Figure 9, illustration 1). As the vapor bubble grows, it moves preferentially to the primary channels parallel to the flow direction (illustration 2). As the heat flux increases, the adjacent bubbles can rapidly coalesce and form an elongated bubble. Besides, the bubbles can easily wrap around the micro-pin fins' edge due to the sharp corner of micro-pin fins, allowing the coalescence with the vapor bubbles in the secondary channel (3).

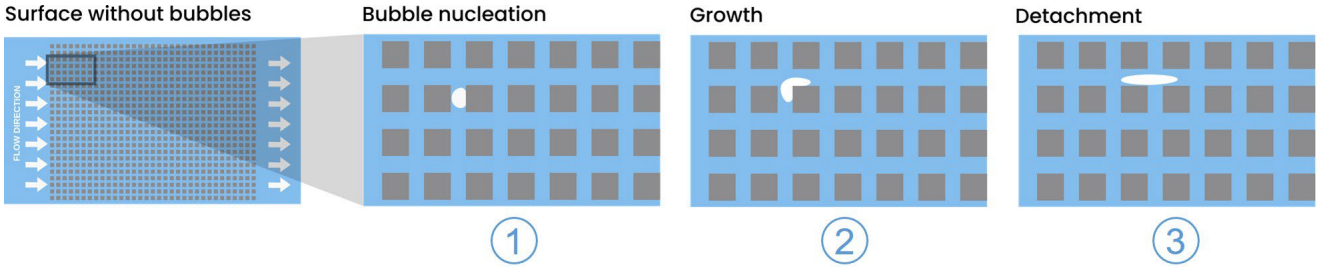

Figure 9. Scheme illustrating bubble nucleation, growth and detachment along the heat sink.

Figure 10 shows the flow visualization for G = 1200 kg/m²s and ΔT_{sub} = 20°C. It is worth mentioning that similar behavior was observed for all test conditions. Videos of flow boiling under these mentioned conditions can be found in the Supplementary Material.

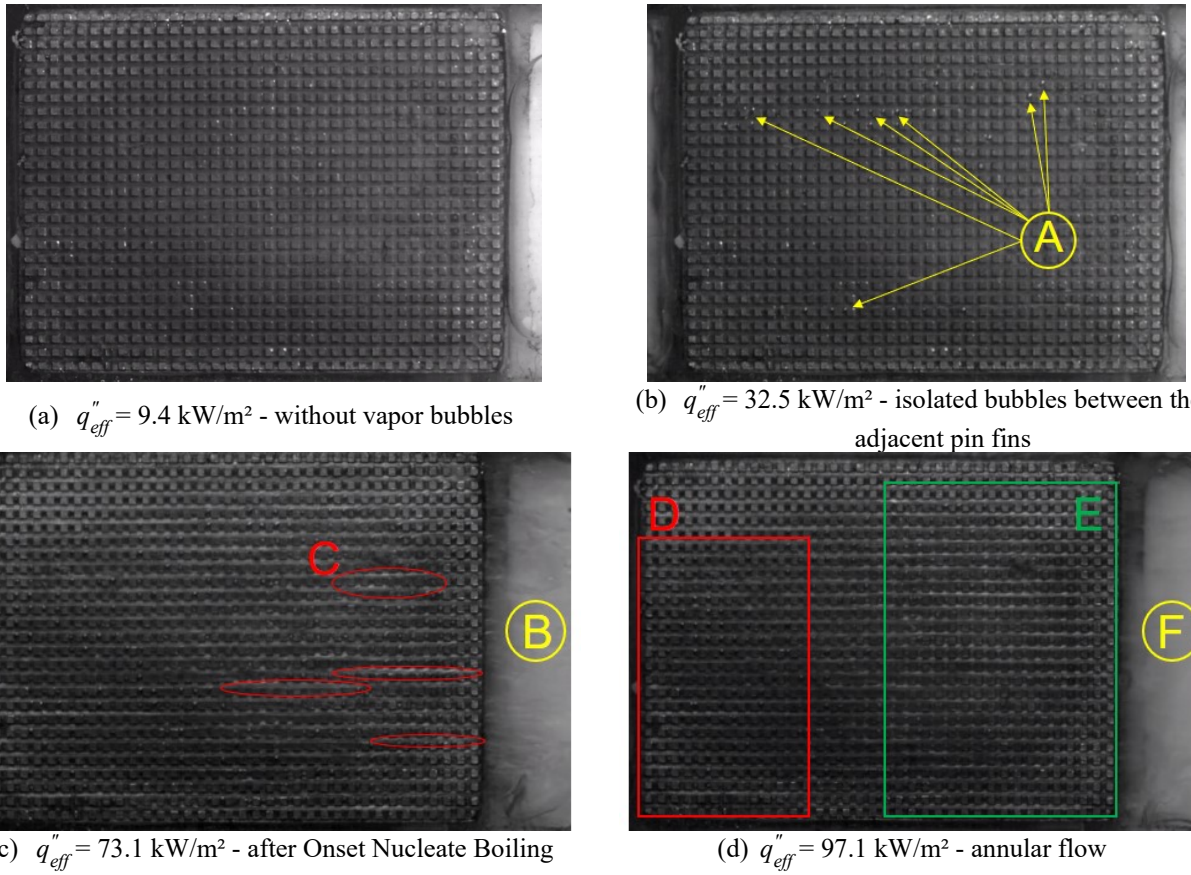

(a) q''_{eff} = 9.4 kW/m² - without vapor bubbles

(b) q''_{eff} = 32.5 kW/m² - isolated bubbles between the adjacent pin fins

(c) q''_{eff} = 73.1 kW/m² - after Onset Nucleate Boiling

(d) q''_{eff} = 97.1 kW/m² - annular flow

Figure 10. High-speed camera images of the micro-finned surface at low, medium, and high heat flux applied. (a) q''_{eff} = 9.4 kW/m²; (b) q''_{eff} = 32.5 kW/m²; (c) q''_{eff} = 73.1 kW/m²; (d) q''_{eff} = 97.1 kW/m².

Initially, at lower heat flux, the single-phase flow regime is predominant, with no vapor bubbles (Figure 10.a). As heat flux increases, isolated vapor bubbles grow preferentially between the adjacent fins (A), even though the working fluid temperature is lower than the saturation temperature at the system pressure - subcooled boiling condition (Figure 10.b). In the saturated boiling region, nucleation sites are activated over the entire heating surface (Figure 10.c), increasing the departure frequency and the coalescence of vapor bubbles near the heat sink outlet (C). Moreover, in

region (B) of Figure 10.c, the amount of vapor increased substantially. For high heat fluxes, the vapor core fills the entire length of the heat sink (Figure 10.d); in this operating condition, the annular flow regime becomes more prominent (E). Near inlet flow, bubbles are formed in the region (D), which coalesce and form the vapor core shown in the region (E). High vapor quality is observed at the region (F), promoting thermal instabilities/fluctuations, increased pressure drop, and appearance of reverse flow mainly observed for lower inlet subcooling temperature.

4. CONCLUSION

This study analyzed the thermal and hydrodynamic behavior of convective flow boiling using HFE-7100 on a heat sink based on square micro-pin fins. Two inlet subcooling temperatures, 10 and 20°C, and three different mass fluxes (800, 1000 and 1200 kg/m²) were analyzed as a function of heat flux. High-speed visualization was performed to explore the transition from single-phase to two-phase flow, identify flow patterns and reverse flow occurrence. Primary findings are summarized as follows:

- ✓ As the mass flux increases, HTC enhancement is observed for the region where the forced convection effects are dominant; when boiling effects overlap, there is no significant increase in HTC with mass flux;
- ✓ For lower inlet subcooling temperature, the ONB occurs at a lower heat flux, and a larger region of the heat sink is filled with vapor, which can accelerate the surface drying process, degrading the HTC for lower heat fluxes compared to higher inlet subcooling temperature.
- ✓ The pressure drop drastically increases with the increase of the vapor amount flowing into the system; such behavior is more pronounced for lower inlet subcooling temperature, leading to the hydrodynamic limit of the system at significantly lower heat fluxes compared to higher inlet subcooling.
- ✓ The reverse flow occurrence was observed, more intensely for ΔT_{sub} = 10 ºC; the high vapor core acts as a barrier to the flow, degrading the HTC, increasing the pressure drop and causing thermal and hydrodynamic instabilities.

5. ACKNOWLEDGEMENTS

The authors are grateful for the financial support from the PPGEM – UNESP/FEIS, from CAPES, from CNPq (grant number 458702/2014-5), and FAPESP (grants numbers 2013/15431-7 and 2019/02566-8). The authors also extend their gratitude to Prof. Dr. Alessandro Roger Rodrigues from Núcleo de Manufatura Avançada da Escola de Engenharia de São Carlos/USP and Prof. Dr. Ricardo Arai from IFSP/São Carlos for their important contribution to this work. Finally, the authors are grateful to Acade Indústria Metalúrgica Eireli for its important contribution for this work.

6. REFERENCES

Asrar, P., Ghiaasiaan, S. M., Joshi, Y. K., 2021. “Two-Phase Heat Transfer and Flow Regimes in Pin Fin-Enhanced Microgaps – Effect of Pin Spacing”. *Journal of Heat Transfer – ASME*, Vol. 143, 023001-1.

Cao, Z., Liu, B., Preger, C., Wu, Z., Zhang, Y., Wang, X., Sundén, B. 2018. “Pool boiling heat transfer of FC-72 on pin-fin silicon surfaces with nanoparticle deposition”. *International Journal of Heat and Mass Transfer*, Vol. 126, p. 1019-1033.

Chalfi, T.Y., Ghiaasiaan, S., 2008. “Pressure drop caused by flow area changes in capillaries under low flow conditions”. *International Journal of Multiphase Flow,* Vol. 34, No. 1, pp. 2 – 12.

Cheng, X., Wu, H., 2021. “Improved flow boiling performance in high-aspect-ratio interconnected microchannels”. *International Journal of Heat and Mass Transfer,* Vol. 165, p. 120627.

Chien, L.H., Cheng, Y.T., Lai, Y.L., Yan, W.M., Ghalambaz, M., 2020. “Experimental and numerical study on convective boiling in a staggered array of micro pin-fin microgap”. *Int. Journal of Heat and Mass Transfer*, Vol. 149. 119203.

Dalkiliç, A. S., Özman, C., Sakamatapan, K., Wongwises, S., 2018 “Experimental investigation on the flow boiling of R134a in a multimicrochannel heat sink”. *International Communications in Heat and Mass Transfer*, Vol. 91, p. 125.

Dang, C., Jia, L., Peng, Q., Yin, L., Qi, Z., 2020. “Comparative study of flow boiling heat transfer and pressure drop of HFE-70 0 0 in continuous and segmented microchannels”. *Int. Journal of Heat and Mass Transfer*, Vol. 148, p. 11903.

Deng, D.; Zeng, L.; Sun, W.; Pi, G.; Yang, Y., 2021. “Experimental study of flow boiling performance of open-ring pin-fin microchannels”. *International Journal of Heat and Mass Transfer*, Vol. 167. 120829.

Dong. L., Quan, X., Cheng, P., 2014. “An experimental investigation of enhanced pool boiling heat transfer from surfaces with micro/nano-structures”. *International Journal of Heat and Mass Transfer*, Vol.71, p. 189-196.

Figliola, R.S. and Beasley, D.E., 2006. *Theory and Design for Mechanical Measurements.* John Wiley & Sons, New Jersey, 4th edition.

Fu, B. R., Lin, P. H., Tsou, M.S., Pan, C., 2012. "Flow pattern maps and transition criteria for flow boiling of binary mixtures in a diverging microchannels". *International Journal of Heat and Mass Transfer*, Vol. 55, p. 1754-1763.

Harirchian, T.; Garimella, S. V., 2008. "A comprehensive flow regime map for microchannel flow boiling with quantitative transition criteria". *International Journal of Heat and Mass Transfer*, Vol. 53, p. 2694–2702.

Jiang, L., Koo, J., Wang, E., Bari, A., Cho, E.S., Ong, W., Prasher, R.S., Maveety, J., Kenny, T.W., Kim, M.S., Santiago, J.G., Goodson, K.E., 2002. "Cross-linked microchannels for VLSI hotspot cooling". In *Proceedings of ASME International Mechanical Engineering Congress and Exposition, IMECE2002*. Louisiana, USA, pp. 13–17.

Kadam, S. T.; Kumar, R., 2014. "Twenty-first-century cooling solution: microchannel heat sinks". *International Journal of Thermal. Sciences*, Vol. 85, p. 73-92.

Kandlikar, S. G., 2016. "Mechanistic considerations for enhancing flow boiling heat transfer in microchannels*". Journal of Heat Transfer, ASME*, Vol. 138(2), 021504.

Kiyomura, I. S., Nunes, J. M., de Souza, R. R., Gajghate, S. S., Bhaumik, S., Cardoso, E. M., 2020. "Effect of microfin surfaces on boiling heat transfer using HFE-7100 as working fluid". *Journal of the Brazilian Society of Mechanical Sciences and Engineering*, *42*(7), 1-13.

Leão, H.L.S.L., Nascimento, F.J. and Ribatski, G., 2014. "Flow boiling heat transfer of r407c in a microchannels based heat spreader". *Experimental Thermal and Fluid Science,* Vol. 59, pp. 140 – 151.

Lee, P.C., Pan, C., 2008. "Boiling heat transfer and two-phase flow of water in a single shallow microchannel with a uniform or diverging cross-section". *Journal of Micromechanics and Microengineering*, Vol. 18.

Manetti, L.L.; Ribatski, G.; Souza, R.R; Cardoso, E.M. 2020. "Pool boiling heat transfer of HFE-7100 on metal foams". *Experimental Thermal and Fluid Science*, v. 113, 110025.

McNeil, D. A.; Raeisi, A. H.; Kew, P. A.; Hamed, R. S., 2014. "An investigation into flow boiling heat transfer and pressure drop in a pin–finned heat sink". *International Journal of Multi-phase Flow*, Vol. 67, p. 65-84.

Mihailovic, M.; Rops, C. M.; Hao, J.; Mele, L.; Creemer, J. F.; Sarro, P. M., 2011. "MEMS silicon-based micro-evaporator". *Journal of Micromechanics and Microengineering*, Vol. 21, p. 075007.

Mukherjee, A.; Kandlikar, S. G., 2005. "Numerical study of the effect of inlet constriction on bubble growth during flow boiling in microchannel". *In Proceedings of 3rd International Conference on Microchannels and Minichannels*, 13 a 15 Junho, Toronto, Canadá.

Power America. Disponível em: <*https://energy.gov/eere/amo/power-america*>. Acessado em 03 jun 2019.

Prajapati, Y. K.; Pathak, M.; Khan, M. K., 2017. "Bubble dynamics and flow boiling characteristics in three different microchannel configurations". *International Journal of Thermal Sciences*, Vol. 112, p. 371-382.

Rahman, M., Olceroglu, O., Mccarthy, M. 2014. "Role of wickability on the critical heat flux of structured superhydrophilic surfaces". *Langmuir*, Vol. 30, n. 37, p. 11225-11234.

Reeser, A.; Bar-Cohen, A.; Hetsroni, G., 2014. "High-Quality Flow Boiling Heat Transfer and Pressure Drop in Microgap Pin Fin Arrays*". International Journal of Heat and Mass Transfer*, Vol. 78, p. 974–985.

Woodcock, C., Yu, X., J. Plawsky, J., Peles, Y., 2015. "Piranha Pin Fin (PPF) –Advanced flow boiling microstructures with low surface tension dielectric fluids". *International Journal of Heat and Mass Transfer,* Vol. 90, p. 591–604.

Xu, J.L., Zhang, W., Wang, Q.W., Su, Q.C., 2006. "Flow instability and transient flow patterns inside intercrossed silicon microchannel array in a micro-timescale". *International Journal of Multiphase Flow*, Vol. 32, p. 568–592.

Yin, L., Chauhan, A., Recinella, A., Jia, L., Kandlikar, S.G., 2020. "Subcooled flow boiling in an expanding microgap with a hybrid microstructured surface". *International Journal of Heat and Mass Transfer,* Vol. 151, p. 119379.

Yin, L., Jiang, P., Xu, R., Hu, H., 2020. "Water flow boiling in a partially modified microgap with shortened micro pin fins". *International Journal of Heat and Mass Transfer,* Vol. 155, p. 119819.

7. RESPONSIBILITY NOTICE

The authors are the only ones responsible for the printed material included in this paper.